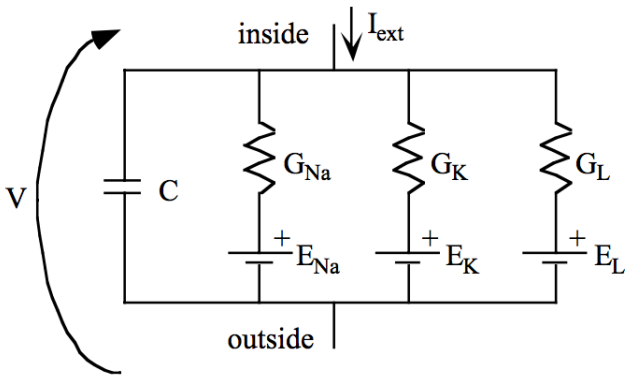

Fig. 1 Typical membrane circuit containing active Na and K channels, a leakage channel and a membrane

$$C\frac{dV}{dt} = I_{ext} - G_{Na}(V - E_{Na}) - G_{K1}(V - E_K) - G_L(V - E_L)$$

$$G_{Na} = \overline{G}_{Na} m^3 h \qquad \frac{dm}{dt} = \frac{m_\infty(V) - m}{\tau_m(V)}$$

$$\frac{dh}{dt} = \frac{h_\infty(V) - h}{\tau_h(V)}$$

$$G_K = \overline{G}_K n^4 \qquad \frac{dn}{dt} = \frac{n_\infty(V) - n}{\tau_n(V)}$$

$$m_\infty(V) = 0.5\left[1 + \tanh\left(\left(V - V_1\right)/V_2\right)\right]$$

$$w_\infty(V) = 0.5\left[1 + \tanh\left(\left(V - V_3\right)/V_4\right)\right]$$

$$\tau_w(V) = \frac{1}{\cosh\left(\left(V - V_3\right)/V_4\right)}$$

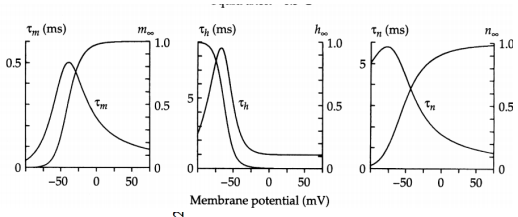

Fig. 2 Parameters of the Hodgkin-Huxley model for squid giant axon membrane.

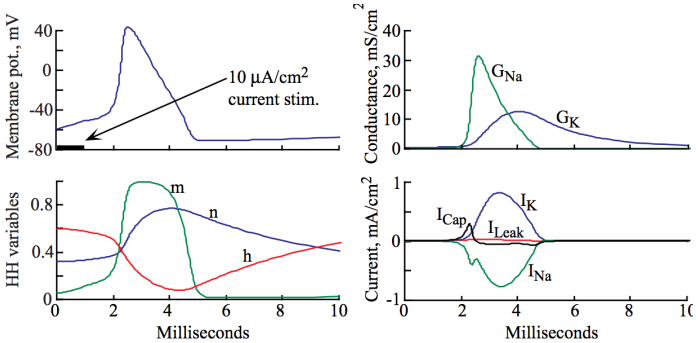

Fig. 3 Time course of the important variables in the HH model for nerve action potentials during an action potential. Shown are the membrane potential (upper left), the HH variables (lower left), the conductances (upper right), and the membrane currents (lower right).

1. For an increasing number of channels, the kinetic scheme of Eqn. 4 has been found to be inaccurate. More complex channel state models are needed and these can now be derived from single channel recordings. This means that explicit differential equations for the state model have to be written and these usually cannot be collapsed into the compact form of the HH equations (Eqn. 2). This change in the model generally reflects subtle changes in the gating behavior of channels.

2. The HH model assumes that the instantaneous current-voltage relationship of a channel is linear, i.e. that $I_x = G_x(V,t)(V - E_x)$. As discussed in the notes on channel permeation models, the current-voltage relationship does not necessarily take this linear form. Usually a more accurate instantaneous current voltage model is the Goldman-Hodgkin-Katz constant field equation:

$$I_i = (\text{const.})\, m^p h^q V \frac{\left[C_{inside}\, e^{z_i FV/RT} - C_{outside}\right]}{e^{z_i FV/RT} - 1} \qquad (5)$$

where m and h are HH variables as in Eqn. 2 and Eqn. 5 is substituted for the linear current voltage relationships in Eqn. 1. Equation 5 is most commonly used in modeling Ca^{++} channels, because the large concentration ratio C_{out}/C_{in} leads to strong rectification. In these notes, the linear form of the equation, i.e. Eqn. 1, will be used for simplicity of analysis.

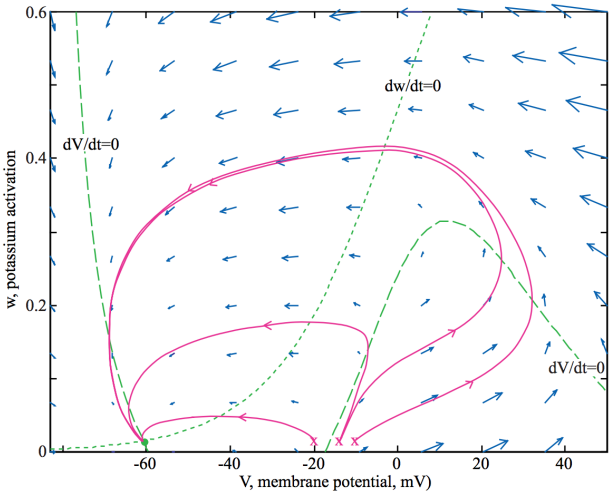

Fig. 5. Phase plane for the MLE with parameter set #1. The green dashed lines are the nullclines *dw/dt*=0 and *dV/dt*=0. The blue arrows show the directions and flow velocities of trajectories at the points corresponding to the tails of the arrows. The magenta solid lines are example trajectories for V_i=-20 mV, -14 mV, -13.9 mV, and –10 mV, respectively from left to right. The corresponding *V* versus time plots are shown in Fig. 6.

$$\frac{dV}{dt} = 0 \quad \Rightarrow \quad w_V(V) = \frac{I_{ext} - \overline{G}_{Ca}\, m_\infty(V)(V - E_{Ca}) - \overline{G}_L(V - E_L)}{\overline{G}_K(V - E_K)}$$

$$\frac{dw}{dt} = 0 \quad \Rightarrow \quad w_w(V) = w_\infty(V)$$

1. Because a derivative is zero on a nullcline, the system is constrained to cross the nullclines moving either horizontally (across the *dw/dt*=0 nullcline) or vertically (across the *dV/dt*=0 nullcline). This can be seen in Fig. 5 by the directions of the arrows and the trajectories near the nullclines.

2. The system's velocity changes direction across the nullclines. Thus, below the *dV/dt* nullcline, the direction of flow along the *V* axis is positive, the blue arrows in Fig. 5 point to the right. Above the *dV/dt* nullcline, the flow is to the left and the blue arrows point leftward. Similarly, below the *dw/dt* nullcline, the flow is upward and above this nullcline, the flow is downward.

The differential equations for the HH parameters m, n, and h are parameterized by rate functions $A_x(t)$ and $B_x(t)$ where:

$$\frac{dm}{dt} = A_m(V)[1 - m] - B_m(V)m \qquad A_m(V) = \frac{\alpha_m(V - V_{cm})}{1 - e^{-(V - V_{cm})/K_{cm}}} \qquad B_m(V) = \beta_m e^{-(V - V_{\beta m})/K_{\beta m}}$$

$$\frac{dh}{dt} = A_h(V)[1 - h] - B_h(V)h \qquad A_h(V) = = \alpha_h e^{-(V - V_{ch})/K_{ch}} \qquad B_h(V) = \frac{\beta_h}{1 - e^{-(V - V_{\beta h})/K_{\beta h}}} \qquad (23)$$

$$\frac{dn}{dt} = A_n(V)[1 - n] - B_n(V)n \qquad A_n(V) = \frac{\alpha_n(V - V_{cn})}{1 - e^{-(V - V_{cn})/K_{cn}}} \qquad B_n(V) = \beta_n e^{-(V - V_{\beta n})/K_{\beta n}}$$

1. **Stable node:** λ_1 and λ_2 both real and negative. In this case the exponentials in Eqn. 16 both decay with time, so the trajectories move smoothly and exponentially toward the equilibrium point. Such an equilibrium point is an attractor for trajectories in its vicinity and may be an attractor for a large part of the phase plane.

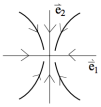

2. **Unstable node:** λ_1 and λ_2 both real and positive. In this case the exponentials in Eqn. 16 both increase without bound, so the trajectories move away from the equilibrium point. The system is stable if placed exactly on such an equilibrium point, but any error will lead to a trajectory that moves away from the equilibrium point.

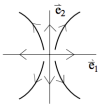

3. **Stable and unstable spiral:** λ_1 and λ_2 both complex; complex eigenvalues must occur in complex conjugate pairs. There are two cases, a stable spiral occurs when the eigenvalues have a negative real part and an unstable spiral occurs when the eigenvalues have a positive real part. The solutions in this case take the form $Ae^{\mathrm{Re}[\lambda]t}\cos(\mathrm{Im}[\lambda]t+\theta)$. The cosine term gives an oscillation at frequency $\mathrm{Im}[\lambda]/2\pi$ whose amplitude grows or shrinks according to the exponential multiplier $\exp(\mathrm{Re}[\lambda]t)$. The sign of $\mathrm{Re}[\lambda]$ determines which. In the phase plane, such solutions will spiral around the equilibrium point, since there is a phase shift between the time waveforms along $\vec{e}_1$ and $\vec{e}_2$. The equilibrium point in Fig. 5 is a stable spiral (the exponential decay is faster than the period of the oscillation in this case, so the spiral is not seen; this case is very similar to a stable node) and Fig. 7 is an unstable spiral.

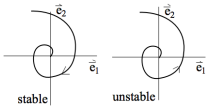

4. **Saddle node**: one real positive eigenvalue and one real negative eigenvalue. The two exponential terms in Eqn. 16 now behave oppositely. One decays exponentially, the other grows exponentially. In the figure at right, λ_1 is negative, so the trajectories decay toward the equilibrium point along the direction of $\vec{e}_1$; λ_2 is positive, so the trajectories move away from the equilibrium point along $\vec{e}_2$. Most trajectories follow a hyperbolic path, as sketched for the four trajectories shown with a single arrowhead. However, there are four trajectories which follow the directions of the eigenvectors $\vec{e}_1$ and $\vec{e}_2$ in the vicinity of the equilibrium point. These are indicated by the double arrowheads in the sketch. These trajectories are produced by initial conditions exactly on one of the eigenvectors, so that there is only one term in Eqn. 16.

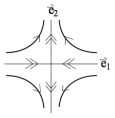

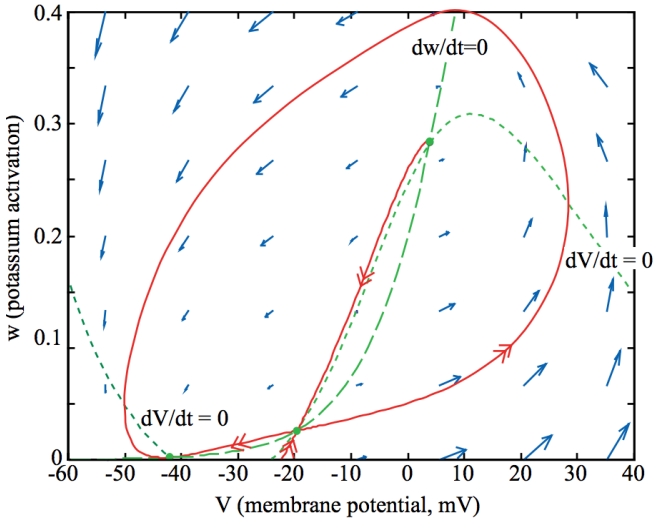

Fig. 8 Phase plane for the MLE with the parameters of set 2. All components are as for Fig. 5 except that the red lines are the stable and unstable manifolds. Note that there are now three equilibrium points (green dots).

1. The stable manifold running vertically downward from the saddle node acts as a true threshold for this system. This fact is apparent from Fig. 9. Consider trajectories from initial values (V_i, w_i) consisting of a depolarized membrane potential V_i and a resting value of the potassium channel state w_i. Such initial conditions lie along a line to the right of the resting potential. The two initial conditions marked with x's in Fig. 9 are on opposite sides of the stable manifold.

   One gives a subthreshold return of membrane potential to rest and one gives an action potential, by following the rightward directed unstable manifold. In this case, initial values to the left of the manifold, by however small an amount, give subthreshold responses and initial values to its right give action potentials. Thus crossing the manifold is the condition for threshold in this system. Furthermore, unlike the action potentials shown in Fig. 5 for parameter set #1, the peak membrane potential of the action potential does not depend on the initial condition, because the action potential trajectories fall very close to the unstable manifold.

2. You should be able to convince yourself, from Fig. 8 and Fig. 9, that there is no limit cycle in this system. Because the membrane potential cannot cross any of the manifolds, there is no way to construct a loop in this phase space that is consistent with the blue arrows.

A sufficient condition for a limit cycle for order 2 systems (only) is provided by the Poincaré-Bendixson Theorem.

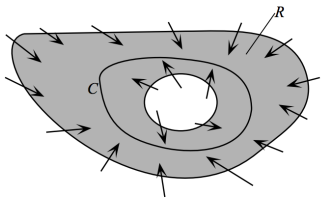

Theorem: Suppose that

1. R is a closed, bounded subset of the plane (shaded at right);
2. $d\vec{x}/dt = \vec{f}(\vec{x})$ is a continuously differentiable vector field on an open set containing R;
3. R does not contain any equilibrium points;
4. There exists a trajectory C that is confined in R, in the sense that it starts in R and stays in R for all time.

Then either C is a closed orbit (limit cycle) or it spirals toward a closed orbit as $t \to \infty$. In either case R contains a closed orbit.

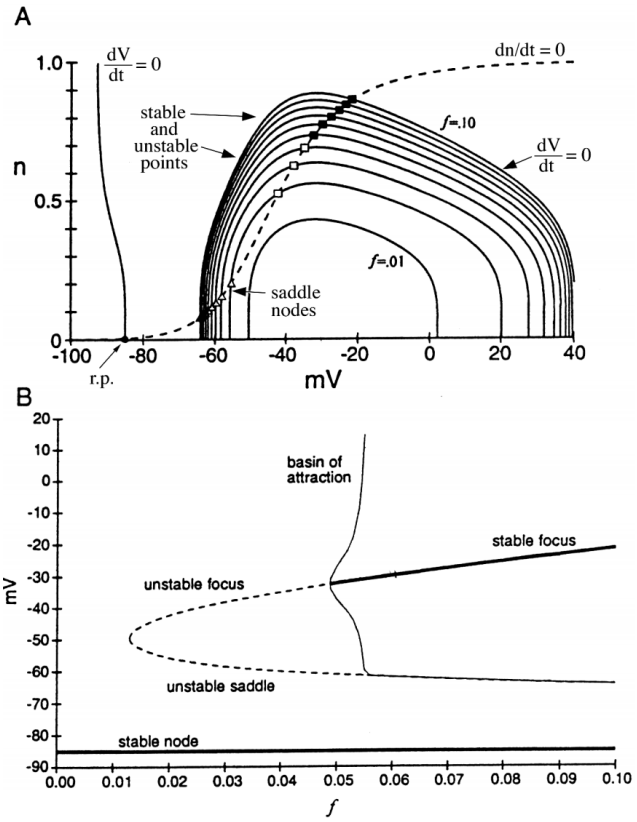

Fig. 17. A. Phase plane for the reduced Cannon et al. model with f varying from 0.01 to 0.1. Shown are nullclines; only the dV/dt=0 nullcline varies with f. Symbols marking equilibrium points vary in shape according to eq. point type. *r.p.* is equilibrium point at resting potential. B. Bifurcation diagram for this system. (modified from Fig. 10 of Cannon et al., 1998.)

Hopf bifurcation

There are several types of bifurcations, of which only the saddle-node variety has been mentioned. A common bifurcation seen in HH systems is a *Hopf bifurcation* which occurs when the eigenvalues of the linearization near an equilibrium point contain a complex conjugate pair. When the real part of the conjugate pair moves from negative (stable spiral) to positive (unstable spiral), the result is a Hopf bifurcation. The change from stable to unstable shown by the third eigenvalue in the reduced Cannon system (at f=0.048) is an example of a Hopf bifurcation. This is not a convenient example for discussion, because the typical bifurcation behavior (emergence of a limit cycle) is actually shown by the negative-time system in this case (i.e. the emergence of the unstable limit cycle). A detailed discussion of Hopf bifurcation can be found in Rinzel and Ermentrout (discussion of Fig. 7.2) and in Strogatz (pp. 248-254).